Supplementary Information

Gate-tuned conductance of graphene-ribbon junctions with nanoscale width variation

Young-Jun Yu[1*†], Jong-Ho Choe[2†], Jong Yun Kim[1], Oh Hun Gwon[1], Hong Kyw Choi[3], Jin Sik Choi[4], Jin Hong Kim[4], Jin-Soo Kim[2], Jin Tae Kim[3], Jun-Hwan Shin[3] and Young Kyu Choi[3]

[1]Department of Physics, Chungnam National University, 99 Daehak-ro, Yuseong-gu, Daejeon, 34134, Korea

[2] Department of Physics, Korea University, Anam-dong 5, Seonbuk-gu, Seoul, 02841, Korea

[3]Electronics and Telecommunications Research Institute (ETRI), 218 Gajeong-ro, Yuseong-gu, Daejeon, 34129, Korea.

[4]Department of Physics, Konkuk University, 120 Neungdong-ro, Gwangjin-gu, Seoul 05029, Korea.

*E-mail: yjyu@cnu.ac.kr

1. Graphene-Ribbon Junction Fabrication

The single-layer graphene field-effect transistors (FETs) were fabricated by mechanical exfoliation on Si wafers covered with ~280-nm thick SiO_2. Then Cr/Au electrodes (0.5 nm/40 nm thickness) were contacted by standard e-beam lithography (see Fig. S1(a)). We employed the e-beam resist of PMMA for defining the dimensions of the GR junction (see Fig. S1(b)). We could isolate the GR junction area from the graphene flakes by etching away the unprotected graphene area between the PMMA etch mask by oxygen plasma (see Fig. S1(c) and (d)).

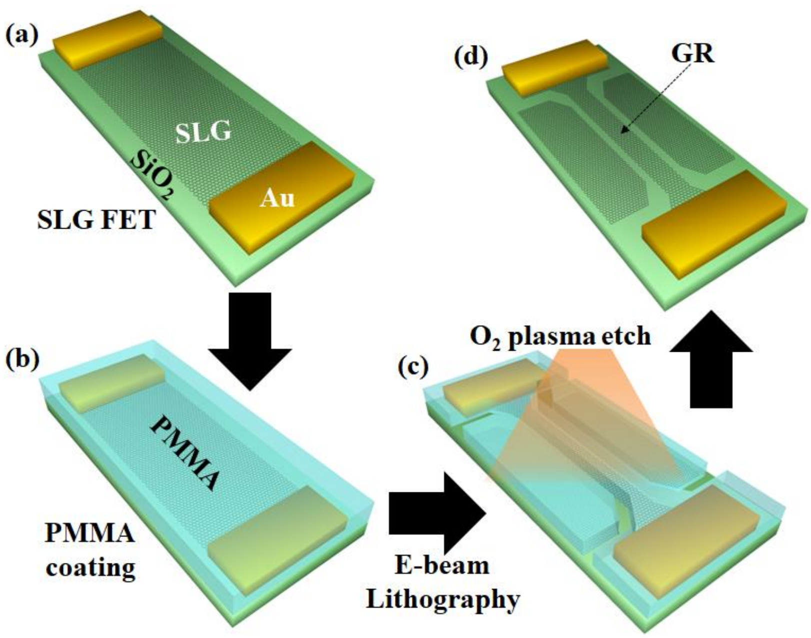

Figure S1. (a)–(d) Schematic diagram for fabrication of GR junction structure from single-layer graphene FET with PMMA e-beam resist as an etch mask, through an oxygen plasma etching process that removes the unprotected graphene.

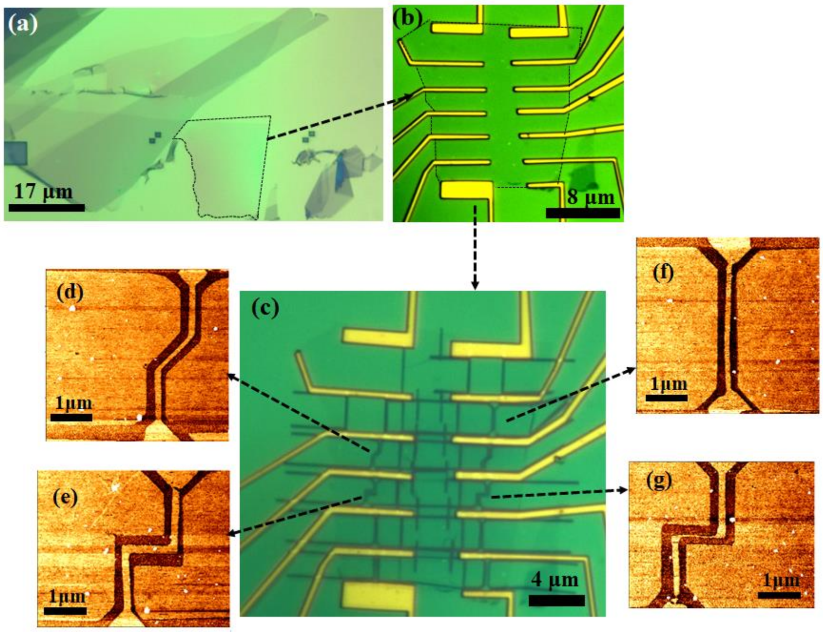

Figure S2. (a) Optical image for mechanically exfoliated single-layer graphene flakes whose shape is marked with a dashed line. (b) Au electrodes in contact with the graphene flake. (c) Optical image of GR junction fabricated from large graphene flake FET. In detail, the developed PMMA mask on the graphene FET flake by e-beam lithography. (d–g) Selected topographic AFM images for various GR junction structures.

2. Electric, EFM, SGM, and SThM data of Graphene-Ribbon Junctions

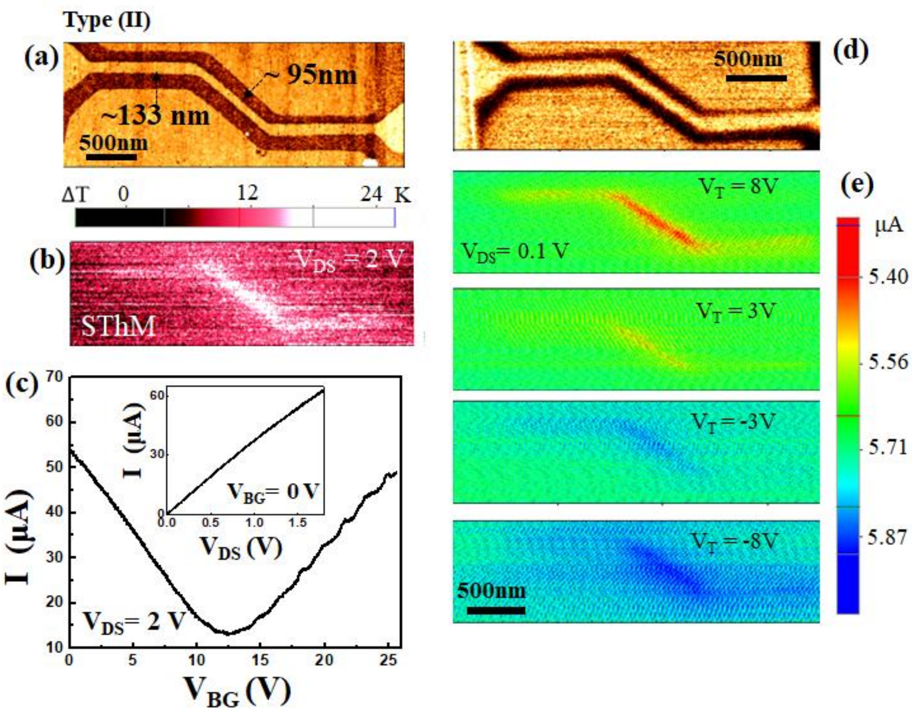

Figure S3. (a) AFM image for type (II) GR junction structure where the straight direction has a ~133 nm wide side GR and 45° path-changed ~95 nm center GR. (b) Thermal image of type (II) GR junction by SThM. (c) Current variation of type (II) GR junction as a function of V_{BG}. Inset: Current variation of type (II) GR junction as a function of V_{DS}. (d) Conductance image of Type (II) GR junction by EFM. (e) SGM images of type (II) GR junction with $V_T = \pm 8$ V or ± 3 V under V_{DS}= 0.1 V.

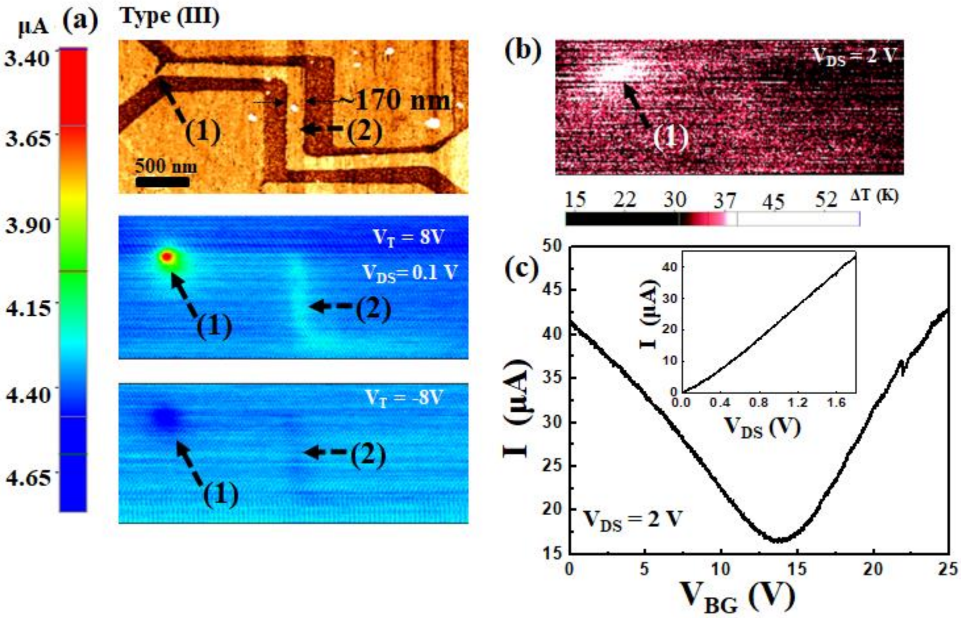

Figure S4. Type (III): 90° path-changed GR junction with ~170 nm width and 1 μm length. The cracked area (marked with (1)) has a width of ~23 nm and was formed during e-beam lithography. (a) AFM (top), SGM (second, third), and (b) SThM images for GR junction. Here, the tip-induced $(I - I_0)/I_0$ of type (III) in Fig. 4(b) was used from position (2) with V_T = 8 V in the second SGM image of (a). (c) Current variation of GR junction as a function of V_{BG}. Inset: Current variation of type (III) GR junction as a function of V_{DS}.

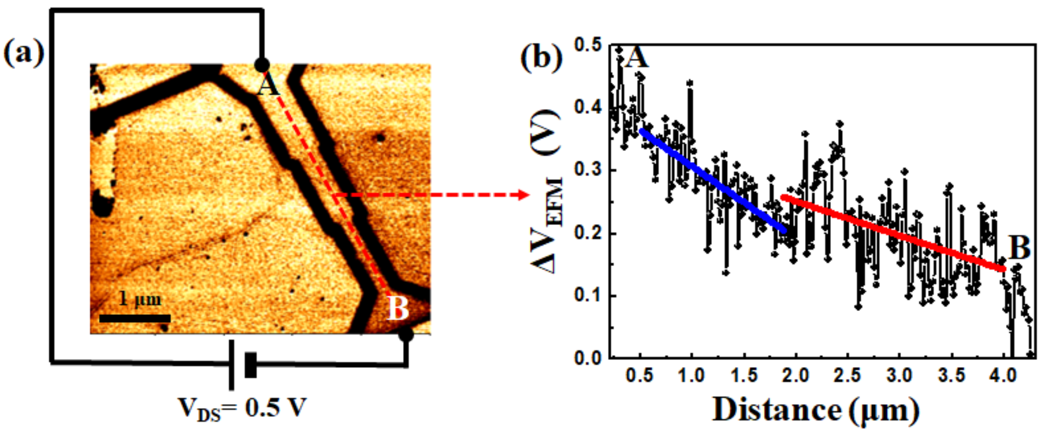

Figure S5. (b) Electric potential difference of GR junction (ΔV_{EFM}) under V_{DS} = 0.5 V, as a function of distance. This ΔV_{EFM} vs distance curve was extracted from along the GR junction between A and B of the EFM image in (a). Here, blue and red lines are linear fitted results for confirming different variations of ΔV_{EFM} for different widths of GR.

3. Numerical Methods and Modeling

(1) Charge Distribution by Electric Field : Simulation of Graphene-Ribbon Under Tip or Back Gating

The 3D modeling of SGM probe gating on the graphene surface can be constructed as shown in Fig. S6.

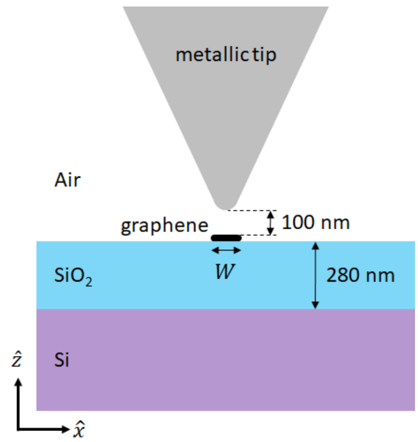

Figure S6. Schematic diagram of 3D simulation of SGM probe gating on graphene surface with a SiO_2/Si substrate. The gating voltage is imposed on the metallic tip region, while Si works as the ground. We set the permittivity of the SiO_2 layer as 3.9. For global back-gating simulation, the metallic tip is removed and the gating voltage is applied to the Si substrate.

The electric potential distribution can be calculated by solving the Maxwell's equation under electrostatic conditions using the boundary element method or finite element method. In this study, we used the COMSOL Multi-Physics software package. We can extracted the gating-induced carrier density (Δn) on the GR from the boundary conditions.

$$\sigma_{top} = \varepsilon_0(\varepsilon_{air}\vec{E}_{air} - \varepsilon_{metal}\vec{E}_{metal})\cdot\hat{z} = \varepsilon_0 E_z \qquad \text{(top)} \qquad (1)$$

$$\sigma_{bottom} = \varepsilon_0(\varepsilon_{metal}\vec{E}_{metal} - \varepsilon_{SiO_2}\vec{E}_{SiO_2})\cdot\hat{z} = -\varepsilon_0\varepsilon_{SiO_2}E_z \qquad \text{(bottom)} \qquad (2)$$

Since the total charge is $\sigma_{total} = \sigma_{top} + \sigma_{bottom}$, the total charge on graphene induced by SGM probe gating voltage V_T is also the same as σ_{total}. This total charge should flow in the GR on the application of the bias voltage V_{DS}, namely, a current I flows. Under gate voltage V_G = 0 V, because the electric field around GR is also zero, current is induced by the impurity charge density in graphene. Note that, owing to too low graphene thickness, we neglected the charge densities on the left and right sides of the graphene. To examine the dependence of the tip position on the tip gating simulation, we located the tip at the center and edge. In Fig. S7, we compare both situations and find that the effect of the tip position is negligible.

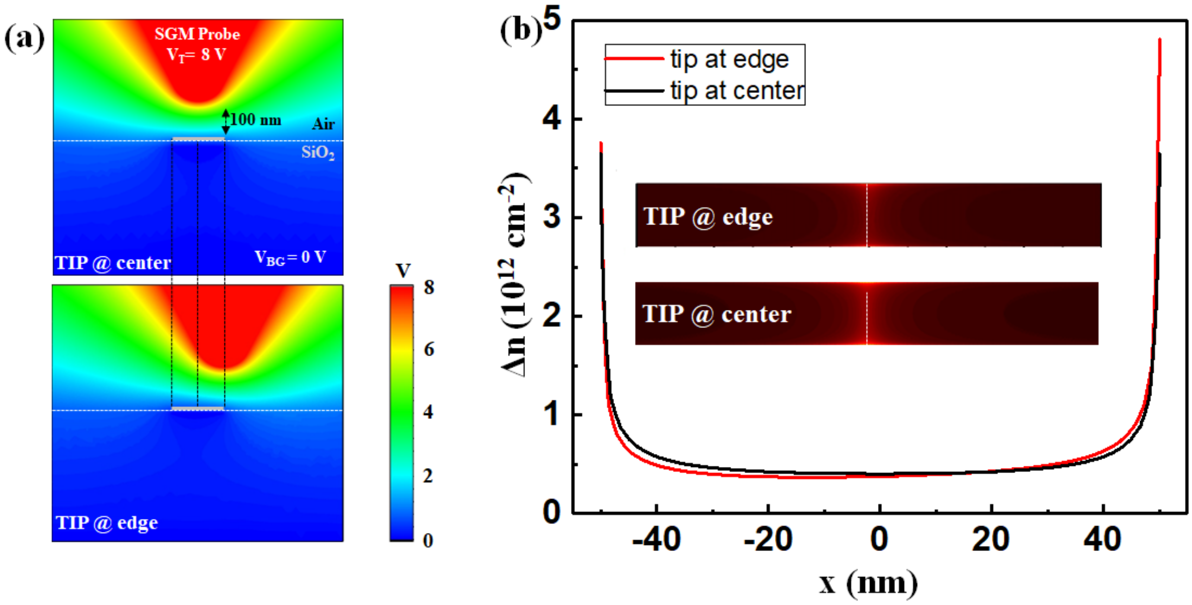

Figure S7. (a) Electric potential distribution of SGM probe with V_T applied on the (top) center or (bottom) edge of the GR on the SiO_2 substrate. (b) Cross-section profiles of Δn along the GR width direction (marked by dashed lines along the x-direction in inset) after the application of V_T at the edge (red line) or center (black line). Inset: Spatial distribution of the carrier density (Δn) induced in GR by applying V_T at the edge or center of GR.

In Fig. S8, we show both back (V_{BG}) and tip (V_T) gating-induced carrier densities (Δn) for various widths (100~500 nm) of GR. These distributions are included in the extraction of the effective conductivity of the GR.

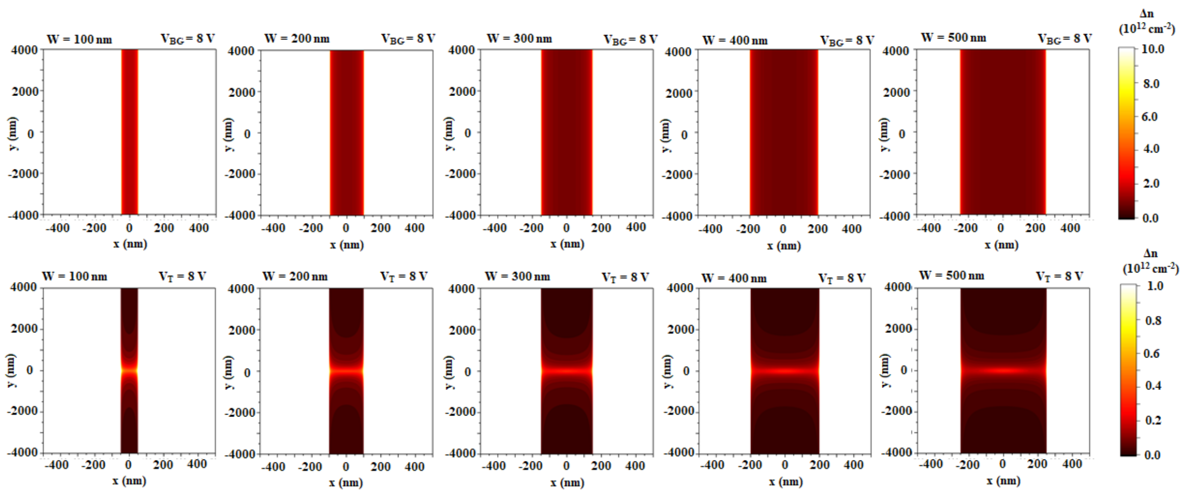

Figure S8. Spatial distribution of the gating-induced carrier density (Δn) for GR with widths ranging from 100 nm to 500 nm by applying either V_T or V_{BG}.

(2) Effective Conductivity of the Graphene-Ribbon with Various Widths

Using the description of local and effective conductivities of graphene (Experimental Section), we calculate the effective conductivity of the graphene ribbon for various widths. We plot the effective conductivity of the GR under back gating (V_{BG} = 8 V) in Fig. S9(a). We also calculate and plot the current variations in the graphene ribbon, depending on the width, assuming the same length of graphene ribbon (see Fig. S9(b)). Here, all $(I - I_0)/I_0$ values in this work are absolute values for comparing the variation as a function of W and global gating.

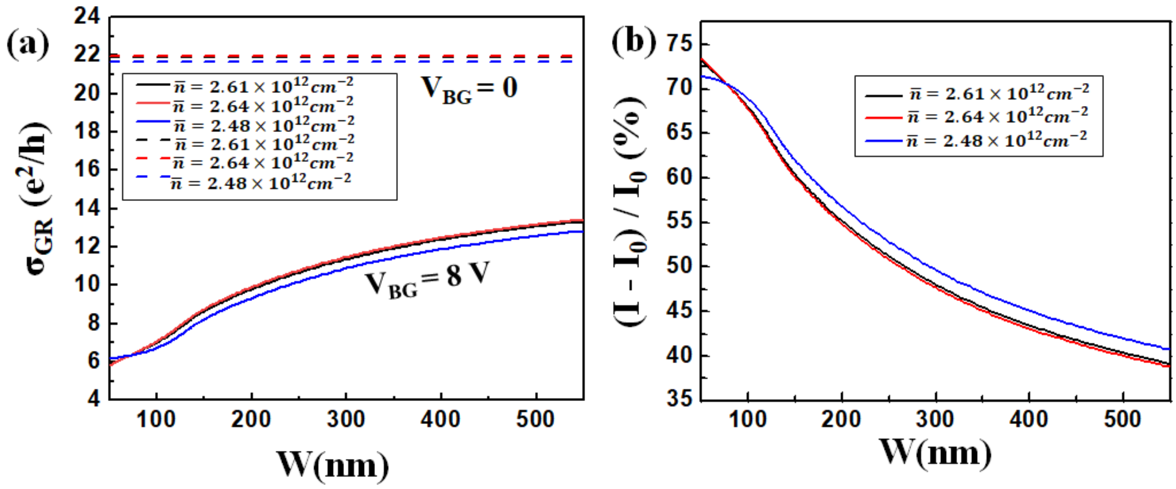

Figure S9. (a) Conductivities of GR (σ_{GR}) as a function of width (W) under application of either V_{BG} = 0 V (dashed lines) or 8 V (solid lines) for various $\bar{n}$ of GR types (I), (II), and (III). (b) Theoretically calculated $(I - I_0)/I_0$ as a function of W under application of V_{BG} = 8 V for various $\bar{n}$ of GR types (I), (II), and (III).

In Fig. S10, we plot the GR conductivities for different widths under tip gating (V_T ~ 8 V) for various $\bar{n}$ of GR types (I), (II), and (III).

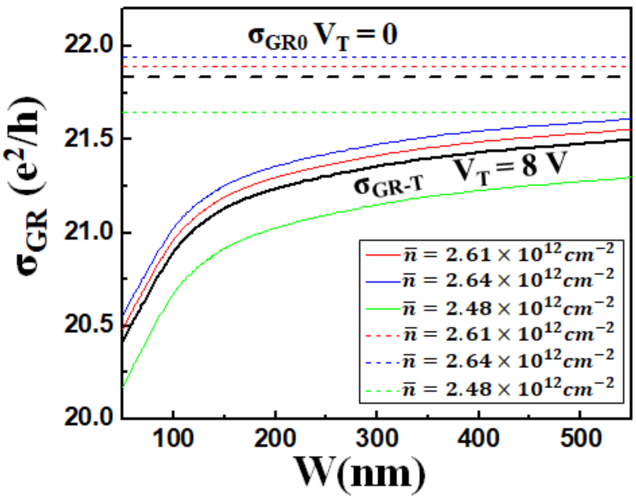

Figure S10. Value of σ_{GR} as a function of W under application of either V_T = 0 V (dashed lines) or 8 V (solid lines) for various $\bar{n}$ of GR types (I), (II), and (III) GR. From these σ_{GR} of GR types (I), (II), and

(III), we averaged the σ_{GR} (black dashed and solid lines), which is exhibited in Fig. 5(a).

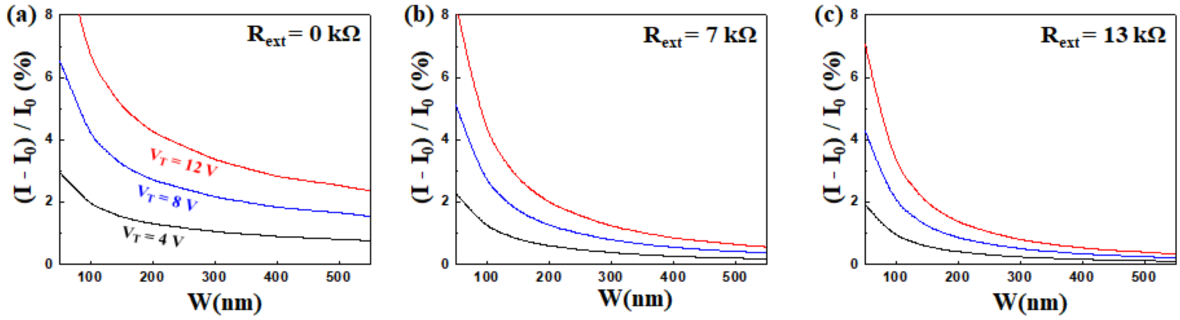

Figure S11. Theoretically calculated current variations around $(I - I_0)/I_0$ as a function of W under application of V_T = 4 V(black lines), 8 V (blue lines), and 12 V (red lines) for R_{ext} = (a) 0 kΩ, (b) 7 kΩ, and (c) 13 kΩ, respectively. Blue lines in (b) and (c) are the same as the dashed lines for R_{ext} = 7 kΩ and 13 kΩ in Fig. 5(b).